Scattering of Guided Modes Caused by an Arbitrarily Shaped Broken End in A Dielectric Slab Waveguide

EIICHI NISHIMURA, STUDENT MEMBER, IEEE, NAGAYOSHI MORITA, MEMBER, IEEE, AND NOBUAKI KUMAGAI, FELLOW, IEEE

Abstract—**Electromagnetic scattering of guided modes in a dielectric slab waveguide caused by an arbitrarily shaped broken end is analyzed theoretically by using the integral equation method. By solving the integral equations iteratively, the tangential components of the electric and magnetic fields on the broken end surface are determined, from which the reflected mode power, the radiation wave power and field patterns, and the total scattered power are obtained. Numerical results are presented for the plane-perpendicular, plane-tilted, and arc-shaped end surfaces. Both TE and TM modes are assumed as an incident wave.**

I. Introduction

RECENTLY, remarkable progress has been made in single-mode fiber techniques, yet several difficult technical problems still remain to be solved before practical single-mode optical fiber transmission systems can be realized. One of the most important problems is the detection and ranging of breakage in the single-mode optical fiber cables. The backscattering method seems to be one of the effective techniques for detecting the fault location and for determining the loss distribution along optical fibers, particularly for the multimode fibers [1]. However, in the case of single-mode fibers, the backscattered power is very small because of the small core diameter and the slight index difference between core and cladding. The method using direct reflected light from breakage is another possible technique for the detection of fault location in the single-mode fibers. The disadvantage of this method is that the amount of reflected power depends strongly on the situations of breakage. Therefore, to discuss the feasibility of this method, we have to know beforehand the reflected power from various types of breakage in the single-mode fibers.

Reflection of guided modes at the tilted-plane end surfaces has been considered in connection with the problems of the imperfectly broken fiber ends [2] and of the tilted mirrors in semiconductor lasers [3]. The theories in these papers, however, are not satisfactory in the sense that they have not taken the full boundary conditions into account. Similar problems have been treated by the variational method [4]–[6] and the mode expansion method [7]. Practically, however, these analyses are applicable only to the vertical end surfaces.

In the present paper, the electromagnetic scattering from the arbitrarily shaped broken ends in a dielectric slab waveguide is analyzed, based on the integral equations which are derived by applying the full boundary conditions on the end surface. In the integral equations, simple, but sufficiently accurate, approximate expressions of the Green's functions are used in the waveguide side, while the conventional Green's function is employed in the external side. Numerical results are presented for the cases of tilted-plane and arc-shaped cut ends of a dielectric slab waveguide embedded in sea water and air for both TE and TM mode incidences. From these numerical data, the possible detectable range of fault location by using reflected pulses from the breakage in the single-mode optical fiber cables can be estimated.

II. Integral Equations

Consider the arbitrarily shaped end surface of the dielectric slab waveguide as shown in Fig. 1. In the figure, c denotes the boundary line between the external side, with refractive index κ_4, and the slab waveguide side, which consists of the core with thickness d and refractive index κ_2, and the upper and lower claddings with refractive indices κ_1 and κ_3, respectively. It is assumed that $\kappa_2 > \kappa_3 \geqslant \kappa_1$.

A. TM Mode Incidence

The tangential field components at a point in the waveguide side and unlimitedly close to the observation point P on c are expressed as [9], [10]

$$H_{sy} = H_y^{\text{inc}} + \int_c \left(H_{sy} \frac{\partial G_H^{ij}}{\partial n'} + j\omega\epsilon_j E_{sv} G_H^{ij} \right) dv' \tag{1}$$

$$E_{sv} = E_v^{\text{inc}} + \int_c \left[jH_{sy} \left(\omega\mu_0 \cos(\beta - \beta') G_H^{ij} - \frac{1}{\omega\epsilon_j} \cdot \frac{\partial^2 G_H^{ij}}{\partial v \partial v'} \right) - E_{sv} \frac{\partial G_H^{ij}}{\partial n} \right] dv' \tag{2}$$

where the subscript H means the case of TM mode inci-

Manuscript received November 17, 1982; revised June 15, 1983. This work was supported in part by a subsidy for research and development on international telecommunications awarded by KDD Engineering and Consulting, Inc. (KEC), Japan.

The authors are with the Department of Communication Engineering, Osaka University, Yamada Oka, Suita 565, Osaka, Japan.

0018-9480/83/1100-0923$01.00 ©1983 IEEE

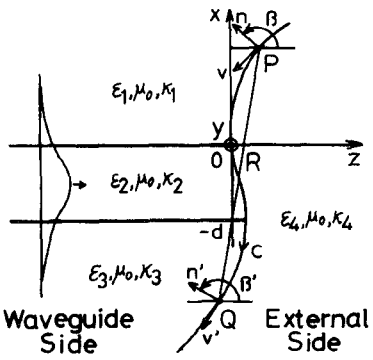

Fig. 1. Profile of arbitrarily shaped broken end in dielectric slab waveguide.

dence, s stands for the slab waveguide side, and j ($j=1,2,3$) refers to the j region (which should not be confused with the imaginary unit). The superscript "inc" denotes the incident fields; G_H^{ij} indicates the Green's function for the waveguide side, where $i(=1,2,3)$ and $j(=1,2,3)$ refer to the regions in which the observation point P and the integration point Q are located, respectively; n, n' and v, v' are the coordinates normal to c and tangential to c, respectively, at the points P and Q on c, while β, β' are the angles between the directions n, n' and the z-axis. The harmonic time dependence $\exp(+j\omega t)$ is assumed and is eliminated throughout the paper. The tangential field components at a point in the external side and unlimitedly close to the point P on c are expressed as

$$H_{ey} = -\int_c \left(H_{ey}\frac{\partial G_4}{\partial n'} + j\omega\epsilon_4 E_{ev} G_4 \right) dv' \tag{3}$$

$$E_{ev} = -\int_c \left[jH_{ey}\left(\omega\mu_0 \cos(\beta-\beta')G_4 - \frac{1}{\omega\epsilon_4}\cdot\frac{\partial^2 G_4}{\partial v\,\partial v'} \right) - E_{ev}\frac{\partial G_4}{\partial n} \right] dv' \tag{4}$$

where the subscript e stands for the external side, and G_4 indicates the Green's function for the infinite domain, i.e.,

$$G_4 = -(j/4)H_0^{(2)}(k_4 R) \tag{5}$$

where $H_0^{(2)}$ is the zeroth-order Hankel function of the second kind, k_i is the wavenumber in the i region ($k_i = \kappa_i k_0 = \omega\sqrt{\epsilon_i\mu_0}$ where $k_0 = \omega\sqrt{\epsilon_0\mu_0}$), and R is the distance between the observation point P and the integration point Q. Let ϕ_{Hs} and ϕ_{He} be

$$\phi_{Hs} = H_{sy}\phi_{He} = H_{ey} \tag{6a}$$

then

$$E_{sv} = \frac{j}{\omega\epsilon_i}\cdot\frac{\partial\phi_{Hs}}{\partial n}, \quad E_{ev} = \frac{j}{\omega\epsilon_4}\cdot\frac{\partial\phi_{He}}{\partial n}. \tag{6b}$$

From the boundary conditions on c, we have the following relations:

$$\phi_{Hs} = \phi_{He}, \quad \frac{1}{\kappa_j^2}\cdot\frac{\partial\phi_{Hs}}{\partial n} = \frac{1}{\kappa_4^2}\cdot\frac{\partial\phi_{He}}{\partial n}. \tag{7}$$

By putting the points, for which (1) and (3) are derived, just on the observation point P on c, and by adding these two equations, we obtain, with the aid of (7)

$$\phi_H = \phi_H^{\text{inc}} + \int_c \left[\phi_H \frac{\partial}{\partial n'}\left(G_H^{ij} - G_4\right) - \frac{1}{\kappa_j^2}\cdot\frac{\partial\phi_H}{\partial n'}\left(\kappa_j^2 G_H^{ij} - \kappa_4^2 G_4\right) \right] dv' \tag{8}$$

where $\phi_H = \phi_{Hs}(=\phi_{He})$. Similarly, by adding κ_i^2 times (2) and κ_4^2 times (4), we obtain

$$\frac{1}{\kappa_i^2}\cdot\frac{\partial\phi_H}{\partial n} = \frac{2}{\kappa_i^2+\kappa_4^2}\cdot\frac{\partial\phi_H^{\text{inc}}}{\partial n} + \frac{2}{\kappa_i^2+\kappa_4^2}\cdot\int_c \left\{ \phi_H \left[k_0^2\cos(\beta-\beta')\left(\kappa_i^2 G_H^{ij} - \kappa_4^2 G_4\right) - \frac{\partial^2}{\partial v\,\partial v'}\left(\frac{\kappa_i^2}{\kappa_j^2}G_H^{ij} - G_4 \right) \right] - \frac{1}{\kappa_j^2}\cdot\frac{\partial\phi_H}{\partial n'}\cdot\frac{\partial}{\partial n}\left(\kappa_i^2 G_H^{ij} - \kappa_4^2 G_4\right) \right\} dv'. \tag{9}$$

Equations (8) and (9) constitute the set of integral equations for ϕ_H and $\partial\phi_H/\partial n$ on c.

B. TE Mode Incidence

Procedure similar to that in the preceding section leads to the following integral equations for the case of TE mode incidence [8]:

$$\phi_E = \phi_E^{\text{inc}} + \int_c \left[\phi_E \frac{\partial}{\partial n'}\left(G_E^{ij} - G_4\right) - \frac{\partial\phi_E}{\partial n'}\left(G_E^{ij} - G_4\right) \right] dv' \tag{10}$$

$$\frac{\partial\phi_E}{\partial n} = \frac{\partial\phi_E^{\text{inc}}}{\partial n} + \int_c \left\{ \phi_E \left[k_0^2\cos(\beta-\beta')\left(\kappa_j^2 G_E^{ij} - \kappa_4^2 G_4\right) - \frac{\partial^2}{\partial v\,\partial v'}\left(G_E^{ij} - G_4\right) \right] - \frac{\partial\phi_E}{\partial n'}\cdot\frac{\partial}{\partial n}\left(G_E^{ij} - G_4\right) \right\} dv' \tag{11}$$

where ϕ_E is the y-component of the electric field on c and the subscript E stands for the case of TE mode incidence.

The range of boundary c need not be extended to infinity, but can be limited to within an appropriate finite extent beyond which the amplitude of the incident fields becomes sufficiently small. The set of integral equations can be transformed by discretization to the matrix equations, which can be solved by means of an iterative procedure provided that the differences of $\kappa_i (i=1, 2, \text{and } 3)$ and κ_4 are very small [8]. The iterative scheme is terminated when the absolute values of the modulus of difference between two successive orders of the values of ϕ and $\partial\phi/\partial n$ become smaller than a certain specified fractional number δ, i.e.,

$$\left|\left(\phi_l^{m+1} - \phi_l^m\right)/\phi_l^{m+1}\right| < \delta \text{ and}$$

$$\left|\left(\partial\phi_l^{m+1}/\partial n - \partial\phi_l^m/\partial n\right)/\left(\partial\phi_l^{m+1}/\partial n\right)\right| < \delta$$

where ϕ_l means the value ϕ on the lth segment (= constant) and m is the iterative number. In the case of TM mode incidence, it is better to use $1/\kappa_i^2 \cdot \partial\phi_H/\partial n$ instead of $\partial\phi_H/\partial n$ as one of the unknowns of (8) and (9).

III. Green's Functions for the Waveguide Side

Although the rigorous Green's function for the waveguide side could be derived, it is extremely complicated and is not suitable for practical computation. Therefore, let us derive the approximate expressions of the Green's function for the waveguide side which are simple enough and yet sufficiently accurate, at least for our practical purposes. Corresponding to the combinations of i and j, i.e., of the regions where the source point Q and the observation point P belong, we use these different types of expressions.

A. The Case Where P and Q are in the Same Region ($i = j$)

In this case, we use the Green's function for the infinite domain

$$G_{E,H}^{ii} = -(j/4)H_0^{(2)}(k_i R). \tag{12}$$

This expression does not take the reflected fields from the waveguide boundaries into account; the contributions of these fields are, however, negligibly small in the present problem, since we have assumed that the refractive index difference between core and cladding is very small [13].

B. The Case Where One Boundary Exists Between P and Q

Let us assume, for instance, that the points Q and P are in the regions of indices κ_1 and κ_2, respectively, as shown in Fig. 2.

When the point Q is not so close to (i.e., more than a few tenths of a wavelength apart from) the boundary, we use the following approximate expression based on geometrical optics [11]:

$$G_{E,H}^{21} = -(j/4)H_0^{(2)}(k_1 L_1)T_{E,H}^{(1)}A^{(1)}e^{-jk_2L_2} \tag{13}$$

with

$$T_E^{(1)} = 2\cos\theta_1/\left(\cos\theta_1 + \sqrt{\epsilon_{12} - \sin^2\theta_1}\right) \tag{14}$$

$$T_H^{(1)} = 2\epsilon_{12}\cos\theta_1/\left(\epsilon_{12}\cos\theta_1 + \sqrt{\epsilon_{12} - \sin^2\theta_1}\right) \tag{15}$$

$$A^{(1)} = \sqrt{ds_1/ds_2}$$
$$= \sqrt{\left(L_1/\kappa_1\cos^2\theta_1\right)/\left[L_1/\left(\kappa_1\cos^2\theta_1\right) + L_2/\left(\kappa_2\cos^2\theta_2\right)\right]} \tag{16}$$

$$\epsilon_{12} = \kappa_2^2/\kappa_1^2. \tag{17}$$

When the point Q comes close to the boundary, the error in (13) increases. For such a case, we use the alternative expression based on an idea of the image method. Applying the boundary conditions at the point K_1 with respect to the fields in the region of κ_1 (which are obtained as the sum of direct and image sources: Fig. 3(a)) and the fields in the region of κ_2 (Fig. 3(b)), we obtain

$$G_{E,H}^{21} = -(j/4)s_{E,H}H_0^{(2)}(k_2 R) \tag{18}$$

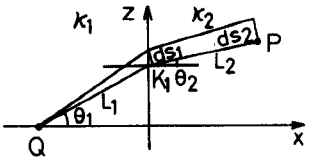

Fig. 2. Treatment by means of the geometrical optics approximation.

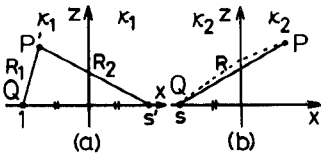

Fig. 3. Image method approach.

with

$$s_E = 2/\left[\frac{H_0^{(2)}(k_2L_1)}{H_0^{(2)}(k_1L_1)} + \frac{\kappa_2}{\kappa_1}\cdot\frac{H_1^{(2)}(k_2L_1)}{H_1^{(2)}(k_1L_1)}\right]$$
$$\simeq 1 - \frac{1}{2}\cdot\frac{\kappa_1-\kappa_2}{\kappa_1}\left[k_1L_1\frac{H_1^{(2)}(k_1L_1)}{H_0^{(2)}(k_1L_1)} - k_2L_1\frac{H_0^{(2)}(k_1L_1)}{H_1^{(2)}(k_1L_1)}\right] \tag{19}$$

$$s_H = 2/\left[\frac{H_0^{(2)}(k_2L_1)}{H_0^{(2)}(k_1L_1)} + \frac{\kappa_1}{\kappa_2}\cdot\frac{H_1^{(2)}(k_2L_1)}{H_1^{(2)}(k_1L_1)}\right]$$
$$\simeq \frac{\kappa_2}{\kappa_1}\left[1 + \frac{1}{2}\cdot\frac{\kappa_1-\kappa_2}{\kappa_1}\left[k_1L_1\frac{H_0^{(2)}(k_1L_1)}{H_1^{(2)}(k_1L_1)} - k_2L_1\frac{H_1^{(2)}(k_1L_1)}{H_0^{(2)}(k_1L_1)}\right]\right]. \tag{20}$$

C. The Case Where Two Boundaries Exist Between P and Q

In this case, we use the approximate expressions similar to that of case *B*.

When the point Q is not so close to the boundary I, we use the following expression based on geometrical optics (Fig. 4):

$$G_{E,H}^{31} = -(j/4)H_0^{(2)}(k_1L_1)T_{E,H}^{(1)}T_{E,H}^{(2)}A^{(1)}A^{(2)}e^{-j(k_2L_2+k_3L_3)} \tag{21}$$

where $T_E^{(1)}$, $T_H^{(1)}$, and $A^{(1)}$ take the same forms as those of (14), (15), and (16), respectively, and

$$T_E^{(2)} = 2\cos\theta_2/\left(\cos\theta_2 + \sqrt{\epsilon_{23} - \sin^2\theta_2}\right) \tag{22}$$

$$T_H^{(2)} = 2\epsilon_{23}\cos\theta_2/\left(\epsilon_{23}\cos\theta_2 + \sqrt{\epsilon_{23} - \sin^2\theta_2}\right) \tag{23}$$

$$A^{(2)} = \sqrt{\left[L_1/\left(\kappa_1\cos^2\theta_1\right) + L_2/\left(\kappa_2\cos^2\theta_2\right)\right]}$$
$$\overline{/\left[L_1/\left(\kappa_1\cos^2\theta_1\right) + L_2/\left(\kappa_2\cos^2\theta_2\right) + L_3/\left(\kappa_3\cos^2\theta_3\right)\right]} \tag{24}$$

$$\epsilon_{23} = \kappa_3^2/\kappa_2^2. \tag{25}$$

When the point Q is close to the boundary I, we use the expression based on both the geometrical optics approxi-

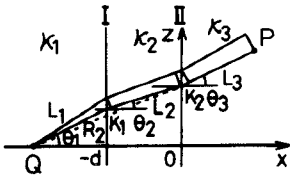

Fig. 4. The case involving two boundaries.

mation and the idea of image method. The result is

$$G^{31}_{E,H} = -(j/4)s_{E,H}H_0^{(2)}(k_2R_2)T^{(2)}_{E,H}A^{(2)}e^{-jk_3L_3} \quad (26)$$

where s_E, s_H and $T_E^{(2)}$, $T_H^{(2)}$ take the same forms as those of (19), (20) and (22), (23), respectively, and $A^{(2)}$ is the same as that of (24).

IV. Scattered Fields

A. Reflected Fields

The reflected fields can be represented by the superposition of guided modes and radiation modes as follows [12]:

$$\mathbf{E}^r = \sum_{\mu=1}^{M} a_\mu^{(-)}\mathbb{E}_\mu + \sum_{\iota=1}^{2}\int_0^{k_3} b_{\rho(\iota)}\mathbb{E}_{\rho(\iota)}\,d\rho \quad (27)$$

$$\mathbf{H}^r = \sum_{\mu=1}^{M} a_\mu^{(-)}\mathbb{H}_\mu + \sum_{i=1}^{2}\int_0^{k_3} b_{\rho(\iota)}\mathbb{H}_{\rho(\iota)}\,d\rho \quad (28)$$

where $a_\mu^{(-)}$ and $b_{\rho(\iota)}$ are the amplitudes of the reflected guided modes and the reflected radiation modes, respectively, ρ denotes the transverse wavenumber of the radiation mode in the lower cladding region, and $(\mathbb{E}_\mu, \mathbb{H}_\mu)$ and $(\mathbb{E}_{\rho(\iota)}, \mathbb{H}_{\rho(\iota)})$ denote the normalized guided and radiation mode fields, respectively. By applying the Lorentz reciprocity theorem for the region surrounded by the contour $c + c_b + c_\infty$ (Fig. 5), we can obtain the amplitude of the reflected modes as follows [13]:

$$a^{(-)}_{E\mu} = \frac{j}{4k_0w_0}\cdot\int_c\left(\phi^*_{E\mu}\frac{\partial\phi^s_E}{\partial n'} - \phi^s_E\frac{\partial\phi^*_{E\mu}}{\partial n'}\right)dv' \quad (29)$$

$$b_{E\rho(\iota)} = \frac{j}{4k_0w_0}\cdot\int_c\left(\phi^*_{E\rho(\iota)}\frac{\partial\phi^s_E}{\partial n'} - \phi^s_E\frac{\partial\phi^*_{E\rho(\iota)}}{\partial n'}\right)dv' \quad (30)$$

$$a^{(-)}_{H\mu} = \frac{jw_0}{4k_0}\cdot\int_c\frac{1}{\kappa_j^2}\left(\phi^*_{H\mu}\frac{\partial\phi^s_H}{\partial n'} - \phi^s_H\frac{\partial\phi^*_{H\mu}}{\partial n'}\right)dv' \quad (31)$$

$$b_{H\rho(\iota)} = \frac{jw_0}{4k_0}\cdot\int_c\frac{1}{\kappa_j^2}\left(\phi^*_{H\rho(\iota)}\frac{\partial\phi^s_H}{\partial n'} - \phi^s_H\frac{\partial\phi^*_{H\rho(i)}}{\partial n'}\right)dv' \quad (32)$$

where $\phi^s = \phi - \phi^{\text{inc}}$, $\partial\phi^s/\partial n = \partial\phi/\partial n - \partial\phi^{\text{inc}}/\partial n$; w_0 is the wave impedance in free space, and * indicates the complex conjugation. The power of the μth reflected guided mode can be obtained from

$$P_\mu = |a_\mu^{(-)}|^2. \quad (33)$$

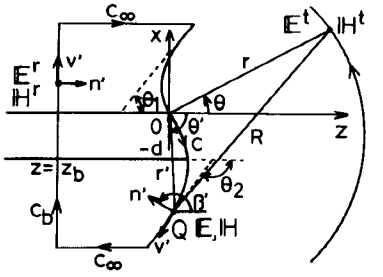

Fig. 5. Illustrative figure used for the calculation of scattered waves.

The reflected radiation fields are given by

$$E_y^r = \sum_{\iota=1}^{2}\int_0^{k_3} b_{E\rho(\iota)}E_{y\rho(\iota)}\,d\rho \quad (34)$$

$$H_y^r = \sum_{\iota=1}^{2}\int_0^{k_3} b_{H\rho(\iota)}H_{y\rho(\iota)}\,d\rho \quad (35)$$

where $E_{y\rho(\iota)}$ and $H_{y\rho(\iota)}$ are the y-components of $\mathbb{E}_{\rho(\iota)}$ and $\mathbb{H}_{\rho(\iota)}$, respectively. The corresponding far-field expressions are obtained by means of the saddle point technique [10]. Let us represent these far fields by $E_y^r(\theta)$ and $H_y^r(\theta)$, where θ is measured from the direction of the positive z-axis. Then, the total reflected radiation power is calculated from

$$P_r = 1/w_0\cdot\left[\int_{\theta_1}^{\pi}\kappa_1|\sqrt{r}\,E_y^r(\theta)|^2\,d\theta + \int_{\pi}^{2\pi-\theta_2}\kappa_3|\sqrt{r}\,E_y^r(\theta)|^2\,d\theta\right] \quad (36)$$

in the case of TE mode incidence, and

$$P_r = w_0/2\cdot\left[\int_{\theta_1}^{\pi}1/\kappa_1|\sqrt{r}\,H_y^r(\theta)|^2\,d\theta + \int_{\pi}^{2\pi-\theta_2}1/\kappa_3|\sqrt{r}\,H_y^r(\theta)|^2\,d\theta\right] \quad (37)$$

in the case of TM mode incidence. In the foregoing equations, θ_1 and θ_2 are the tilt angles of the upward and downward asymptotic lines of c, respectively. If $\theta_1 \simeq \pi/2$ and $\theta_2 \simeq \pi/2$, P_r can be calculated from the following simpler equation:

$$P_r = \sum_{\iota=1}^{2}\int_0^{k_3}|b_{\rho(\iota)}|^2\,d\rho. \quad (38)$$

B. Transmitted Fields

The transmitted far fields, and the total transmitted powers, are given, respectively, as

$$E_y^t(\theta) = \int_c\left(\frac{\partial\phi_E}{\partial n'}G_4 - \phi_E\frac{\partial G_4}{\partial n'}\right)dv' \simeq \frac{1}{4}\sqrt{\frac{2}{\pi k_4 r}}\,e^{-j(k_4r+\pi/4)}\cdot\int_c\left[\frac{\partial\phi_E}{\partial n'} - jk_4\phi_E\cos(\theta-\beta')\right]e^{jk_4r'\cos(\theta-\theta')}\,dv' \quad (39)$$

$$P_t = \kappa_4/(2w_0)\int_{-\theta_2}^{\theta_1}|\sqrt{r}\,E_y^t(\theta)|^2\,d\theta \quad (40)$$

for the case of TE mode incidence, and

$$H_y^t(\theta) = \int_c \left(\frac{\kappa_4^2}{\kappa_j^2} \cdot \frac{\partial \phi_H}{\partial n'} G_4 - \phi_H \frac{\partial G_4}{\partial n'} \right) dv'$$

$$\simeq \frac{1}{4} \sqrt{\frac{2}{\pi k_4 r}}\, e^{-j(k_4 r + \pi/4)}$$

$$\cdot \int_c \left[\frac{\kappa_4^2}{\kappa_j^2} \cdot \frac{\partial \phi_H}{\partial n'} - jk_4 \phi_H \cos(\theta - \beta') \right] e^{jk_4 r' \cos(\theta - \theta')}\, dv' \tag{41}$$

$$P_t = w_0/(2\kappa_4) \int_{-\theta_2}^{\theta_1} |\sqrt{r}\, H_y^t(\theta)|^2\, d\theta \tag{42}$$

for the case of TM mode incidence.

The total scattered power is given by

$$P_s = \sum_{\mu=1}^{M} P_\mu + P_r + P_t \tag{43}$$

both in the cases of TE and TM mode incidences. According to the law of energy conservation, P_s should become equal to the incident mode power.

V. Numerical Results

In this section, the numerical examples of reflected guided and radiation powers, transmitted power, far-field pattern, etc., will be presented for the cases of plane-tilted and arc-shaped end surfaces.

The choice of the Green's functions given in Section III-B and -C, is made as follows: (18) and (26) (for which the idea of image method was applied) are used when the distance from the source point Q to the boundary is less than 0.3 times the wavelength in the corresponding regions; otherwise (13) and (21) are used. The differentiation of (18) and (26) is obtained numerically, while that of (13) and (21) is obtained analytically. The range of integration over c is limited to within the region in which more than 99.98 percent of the power of the highest possible guided mode is contained. The division number in the discretization of an integral is chosen so that the length of each section is about 0.1 times the wavelength in the core or cladding regions (according to the region considered). These values were determined on the basis of numerical evaluation of the convergence feature that was fully done in [8] for the case of the vertical plane end. The accuracy attained varies with the shape of the end surface, waveguide parameters (κ_i; $i = 1 \sim 3$ and d), the types of incident mode (TE or TM), the medium of the external space, etc. One of the simple ways for checking the accuracy of the present method is to evaluate the value of total scattered power P_s (which should be equal to the incident power).

First, let us compare the results of the present method with those of other methods. Fig. 6 shows a comparison with the results of Ikegami [4] and Gelin *et al.* [7], and Table I shows a comparison with the results of Rozzi *et al.* [5]; the numerical values of the parameters used are shown in the corresponding figure and table. For these examples, the direct matrix inversion was used instead of iteration to solve the integral equation set. The results of Fig. 6 and Table I show that the present method is applicable with considerably high accuracy to the cases of a comparatively large refractive index difference.

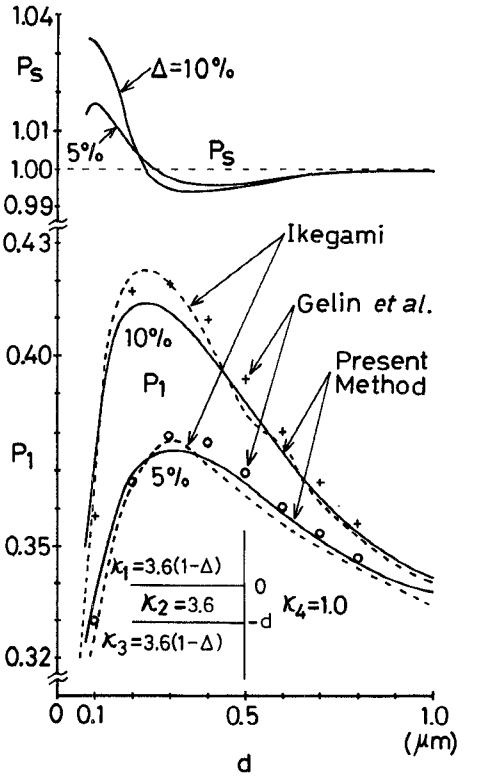

Fig. 6. Comparison of P_1 with that of other methods [4], [7]: P_1 (TE mode incidence, $\lambda_0 = 0.86\mu$m, vertical plane end. Ps: present method only.)

TABLE I
Comparison with Other Method [5]: $a_{1,3}^{(-)}$
$\kappa_1 = \kappa_3 = 3.4$, $\kappa_2 = 3.61$, $\kappa_4 = 1.0$, $\lambda_0 = 0.9\mu$m, $d = 1.6\mu$m, vertical plane end.

incident mode No.		Present Method	Rozzi et al.
1	$a_1^{(-)}$	0.575+j0.001	0.575+j0.003
	$a_3^{(-)}$	-0.004+j0.001	-0.004+j0.002
3	$a_1^{(-)}$	-0.003+j0.002	-0.004+j0.002
	$a_3^{(-)}$	0.663+j0.010	0.660+j0.018

Next, let us assume the waveguide parameters as follows:

$$\kappa_1 = \kappa_3 = 1.5,\ \kappa_2 = 1.515, \text{ and } k_0 d = 14\pi/3.$$

Then, the normalized frequency V becomes about 3.12 and a single guided mode is supported, and about 84 percent of the mode power is confined within the core region in both TE and TM cases. κ_4 is chosen as 1.34 and 1.0, corresponding to sea water and air, respectively. For these examples, the iteration procedure was used to solve the integral equation set, using 10^{-3} as the criterion number δ for the termination of the iterative scheme; the iteration numbers were around 10 for the case of sea water and around 20 for the case of air.

A. Plane Surface End

Figs. 7–10 show the reflected guided mode power P_1, the reflected radiation power P_r, the transmitted power P_t, and the total scattered power P_s as a function of the tilt angle α.

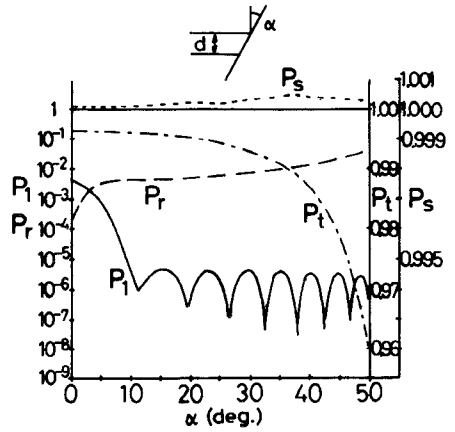

Fig. 7. Reflected guided mode power P_1, reflected radiation power P_r, transmitted power P_t, and total scattered power P_s. (TE mode incidence, $\kappa_4 = 1.34$.)

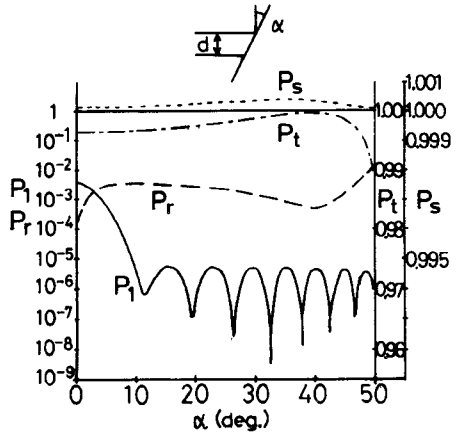

Fig. 8. Reflected guided mode power P_1, reflected radiation power P_r, transmitted power P_t, and total scattered power P_s. (TM mode incidence, $\kappa_4 = 1.34$.)

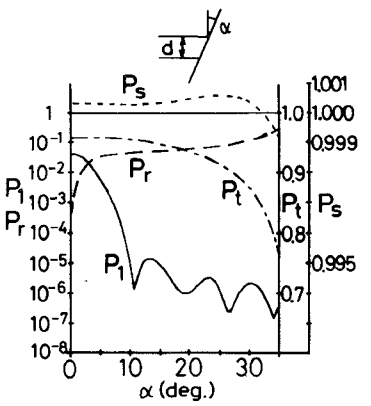

Fig. 9. Reflected guided mode power P_1, reflected radiation power P_r, transmitted power P_t, and total scattered power P_s. (TE mode incidence, $\kappa_4 = 1.0$.)

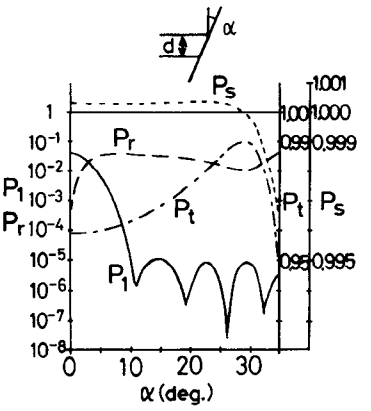

Fig. 10. Reflected guided mode power P_1, reflected radiation power P_r, transmitted power P_t, and total scattered power P_s. (TM mode incidence, $\kappa_4 = 1.0$.)

Figs. 7 and 9 are for the TE mode incidence and Figs. 8 and 10 are for the TM mode incidence. The refractive index in the external side is $\kappa_4 = 1.34$ (sea water) or $\kappa_4 = 1.0$ (air). For the tilt angle α less than about 10°, P_1 decreases monotonically as α increases, while it oscillates for α larger than 10°. At the tilt angles $\alpha \simeq 40°$ in Fig. 8 and $\alpha \simeq 30°$ in Fig. 10, a local maximum appears in the curve of transmitted power P_t and a local minimum appears in the curve of reflected radiation power P_r. It is interesting to note that these angles coincide with the Brewster's angles of the plane wave approximation (41.6° for $\kappa_4 = 1.34$ and 33.5° for $\kappa_4 = 1.0$, when the effective index $\kappa_{\text{eff}} = 1.510$ is used in the waveguide side).

Figs. 11–14 show the typical radiated far-field patterns (note that the scales for the reflected field and the transmitted field are different). It can be seen that, in the case of TE mode incidence, a single lobe appears in the direction of reflection, while in the case of TM mode incidence, two noticeable lobes appear in the different directions. The lobes of the transmission fields point to the 5.9° direction in the case of $\kappa_4 = 1.34$, and to the 17.9° direction in the case of $\kappa_4 = 1.0$. It should be pointed out that these directions are very close to those for the plane wave approximation (6.40° in the case of $\kappa_4 = 1.34$ and 19.0° in the case of $\kappa_4 = 1.0$).

The typical numerical values of P_1, P_r, P_t, and P_s are tabulated in Table II for the cases of $\kappa_4 = 1.34$ ($\alpha = 0°$ and 40°) and $\kappa_4 = 1.0$ ($\alpha = 0°$ and 30°). The values in the parentheses show the corresponding values obtained by means of the plane wave approximation. As far as the principal reflected power is concerned, the results obtained by the plane wave approximation agree well with those obtained by the present analysis except for the case where the TM mode is incident upon a tilted-plane surface end.

B. Arc-Shaped End

Figs. 15–18 show P_1, P_r, P_t, and P_s as a function of the parameter b, which represents the height or depth of an arc-shaped protrusion or depression in the core region. The minus value in b indicates a retracted arc-shape.

VI Discussions and Conclusions

Reflection, transmission, and radiation of the guided mode caused by the arbitrarily shaped broken end in a dielectric slab waveguide were analyzed theoretically by means of the integral equation method. Numerical results were presented for the plane-tilted and the arc-shaped end surfaces. Simple, but sufficiently accurate, approximate Green's functions were derived and utilized to treat the problem.

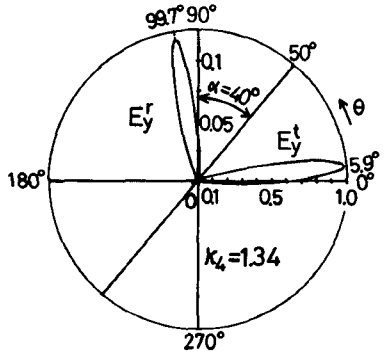

Fig. 11. Radiated far field pattern. (TE mode incidence, $\kappa_4 = 1.34$, $\alpha = 40°$.)

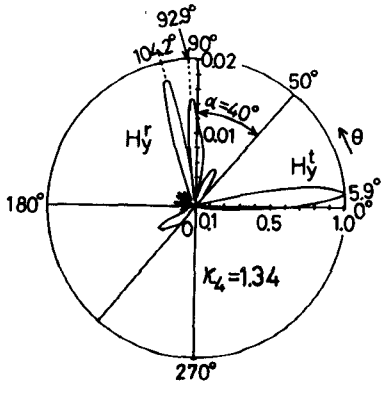

Fig. 12. Radiated far field pattern. (TM mode incidence, $\kappa_4 = 1.34$, $\alpha = 40°$.)

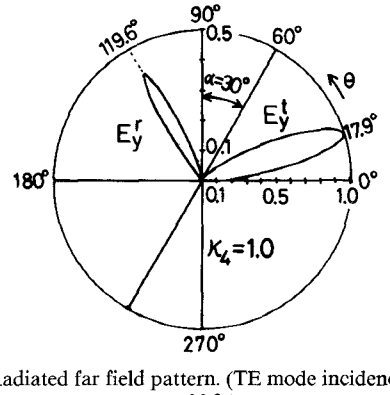

Fig. 13. Radiated far field pattern. (TE mode incidence, $\kappa_4 = 1.0$, $\alpha = 30°$.)

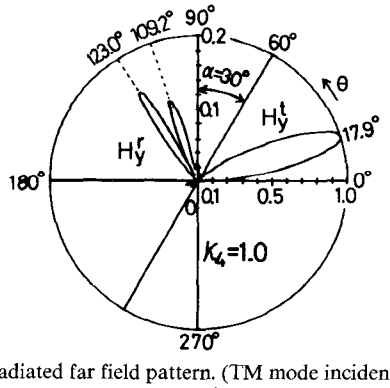

Fig. 14. Radiated far field pattern. (TM mode incidence, $\kappa_4 = 1.0$, $\alpha = 30°$.)

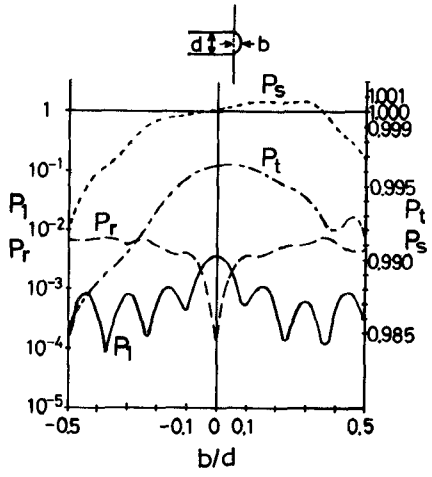

Fig. 15. Scattered powers from the arc-shaped end. The case of $b < 0$ means the retracted arc-shape. (TE mode incidence, $\kappa_4 = 1.34$.)

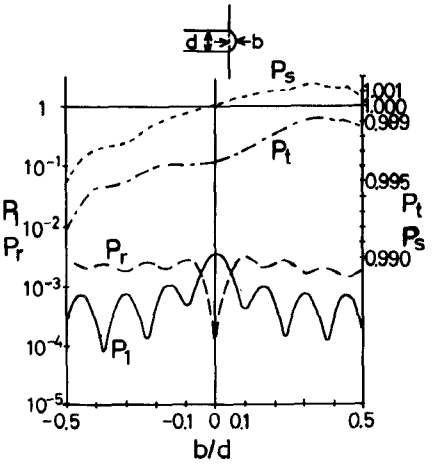

Fig. 16. Scattered powers from the arc-shaped end. The case of $b < 0$ means the retracted arc-shape. (TM mode incidence, $\kappa_4 = 1.34$.)

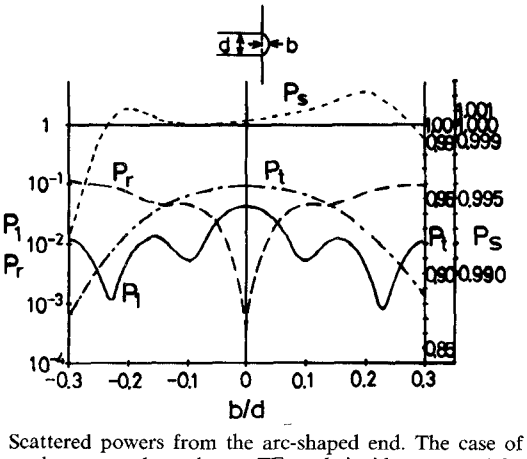

Fig. 17. Scattered powers from the arc-shaped end. The case of $b < 0$ means the retracted arc-shape. (TE mode incidence, $\kappa_4 = 1.0$.)

TABLE II
TYPICAL NUMERICAL VALUES OF P_1, P_r, P_t, AND P_s FOR THE PLANE SURFACE END

κ_4	α°	mode	P_1	P_1 (dB)	P_r	P_t	P_s
1.34	0	TE	$3.68\cdot10^{-3}$ ($3.54\cdot10^{-3}$)	-24.3	$1.22\cdot10^{-4}$	0.99629	1.00000
		TM	$3.65\cdot10^{-3}$ ($3.54\cdot10^{-3}$)	-24.4	$1.25\cdot10^{-4}$	0.99635	1.00013
	40	TE	$3.44\cdot10^{-6}$	-54.6	$1.367\cdot10^{-2}$ ($1.25\cdot10^{-2}$)	0.98674	1.00041
		TM	$4.76\cdot10^{-6}$	-53.2	$4.78\cdot10^{-4}$ ($4.98\cdot10^{-5}$)	0.99988	1.00036
1.0	0	TE	$4.205\cdot10^{-2}$ ($4.12\cdot10^{-2}$)	-13.8	$2.41\cdot10^{-4}$	0.95806	1.00035
		TM	$4.120\cdot10^{-2}$ ($4.12\cdot10^{-2}$)	-13.9	$2.06\cdot10^{-4}$	0.95892	1.00033
	30	TE	$2.17\cdot10^{-6}$	-56.6	0.12331 (0.110)	0.87706	1.00037
		TM	$8.28\cdot10^{-6}$	-50.8	$1.056\cdot10^{-2}$ ($4.48\cdot10^{-3}$)	0.98931	0.99988

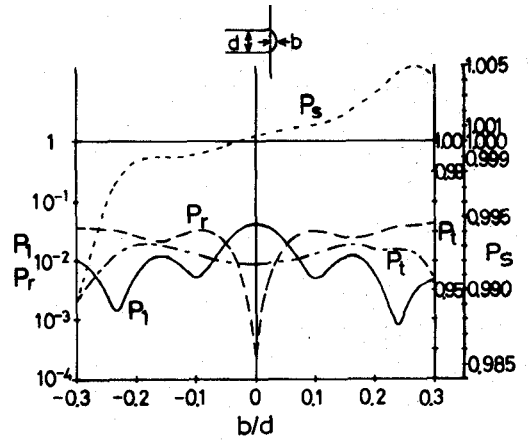

Fig. 18. Scattered powers from the arc-shaped end. The case of $b < 0$ indicates a retracted arc-shape. (TM mode incidence, $\kappa_4 = 1.0$.)

Although we have considered the slab-type waveguides, we would be able to apply these results, at least in order of magnitude, to the cases of optical fiber cables. Our numerical results suggest that the reflected power level larger than -50 dB can be expected, except for the plane surface end with considerably large tilt angles. On the other hand, the backscattered power level evaluated by the theory used in [1] becomes about -50 dB for the optical fiber whose core radius is 3.6 μm, with core and cladding indices being 1.515 and 1.5, respectively, assuming that the wavelength is 1.55 μm ($V \simeq 3.10$), Rayleigh scatter loss is 0.18 dB/km, and pulse duration time is 1 μs. Compared with this result, the method using direct reflected pulse seems to be competitive with the backscattering method for the purpose of detection and ranging of fault location in the single-mode optical fibers.

The method of analysis given in the present paper would be applicable, for instance, to the analysis of the coupling between a laser diode and a dielectric waveguide, and to the analysis of mode coupling of two dielectric waveguides at a joint with tilt and/or offset in the guide axes.

References

[1] K. Aoyama, K. Nakagawa, and T. Itoh, "Optical time domain reflectometry in a single-mode fiber," *IEEE J. Quantum Electron.*, vol. QE-17, pp. 862–868, June 1981.

[2] D. Marcuse, "Reflection losses from imperfectly broken fiber ends," *Appl. Opt.*, vol. 14, pp. 3016–3020, Dec. 1975.

[3] K. Iga, K. Wakao, and T. Kunikane, "Mode reflectivity of tilted mirrors in semiconductor lasers with etched facets," *Appl. Opt.*, vol. 20, pp. 2367–2371, July 1981.

[4] T. Ikegami, "Reflectivity of mode at facet and oscillation mode in double-heterostructure injection lasers," *IEEE J. Quantum Electron.*, vol. QE-8, June 1972.

[5] T. E. Rozzi and G. H. in't Veld, "Variational treatment of the diffraction at the facet of d. h. lasers and of dielectric millimeter wave antennas," *IEEE Trans. Microwave Theory Tech.*, vol. MTT-28, pp. 61–73, Feb. 1980.

[6] M. A. A. Pudensi and L. G. Ferreira, "Method to calculate the reflection and transmission of guided waves," *J. Opt. Soc. Amer.*, vol. 72, no. 1, pp. 126–130, Jan. 1982.

[7] P. Gelin, M. Petenzi, and J. Citerne, "Rigorous analysis of the scattering of surface waves in an abruptly ended slab dielectric waveguide," *IEEE Trans. Microwave Theory Tech.*, vol. MTT-29, pp. 107–114, Feb. 1981.

[8] E. Nishimura, N. Morita, and N. Kumagai, "Theoretical treatment of arbitrarily shaped cut-ends of dielectric optical waveguide," *Trans. IECE Japan*, vol. J65-C, pp. 537–544, July 1982.

[9] N. Morita, "Surface integral representations for electromagnetic scattering from dielectric cylinders," *IEEE Trans. Antennas Propagat.*, vol. AP-26, pp. 261–266, Mar. 1978.

[10] T. Nobuyoshi, N. Morita, and N. Kumagai, "Scattering and mode conversion of guided modes in an optical slab waveguide caused by a cylindrical obstacle of arbitrary cross section shape," *Trans. IECE Japan*, vol. J65-C, pp. 88–95, Feb. 1982.

[11] L. B. Felsen and N. Marcuvitz, *Radiation and Scattering of Waves*. Englewood Cliffs, NJ: Prentice-Hall, 1973, sec. 5.5.

[12] D. Marcuse, *Theory of Dielectric Optical Waveguides*. New York: Academic Press, 1974, ch. 1.3.

[13] N. Morita and N. Kumagai, "Scattering and mode conversion of guided modes by a spherical object in an optical fiber," *IEEE Trans. Microwave Theory Tech.*, vol. MTT-28, pp. 137–141, Feb. 1980.

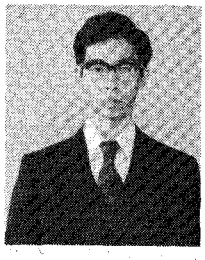

Eiichi Nishimura (S'81) was born in Osaka, Japan, on April 5, 1956. He received the B.S. degree in communication engineering from the Osaka Electro-Communication University, Neyagawa, Osaka, Japan, in 1980, and the M.S. degree in communication engineering from Osaka University, Suita, Osaka, Japan, in 1982. He is currently working toward the Ph.D. degree at Osaka University, where his field of interest is the scattering of electromagnetic waves.

Nagayoshi Morita (M'67) was born in Toyama, Japan, on March 28, 1942. He received B.S., M.S., and Ph.D. degrees in engineering from Osaka University, Suita-shi, Japan, in 1964, 1966, and 1977, respectively.

Since 1966, he has been with the Department of Communication Engineering, Osaka University, Suita-shi, Japan, where he has been engaged in research work on discontinuities in millimeter waveguides and optical waveguides, analytic and numerical techniques for electromagnetic wave problems, bioelectromagnetics, etc.

Dr. Morita is a member of the Institute of Electronics and Communication Engineers of Japan, and Japan Society of Medical Electronics and Biological Engineering.

Nobuaki Kumagai (M'59–SM'71–F'81) was born in Ryojun, Japan, on May 19, 1929. He received the B. Eng. and D. Eng. degrees from Osaka University, Osaka, Japan, in 1953 and 1959, respectively.

From 1956 to 1960, he was a Research Associate in the Department of Communication Engineering at Osaka University. From 1958 through 1960, he was a Visiting Senior Research Fellow at the Electronics Research Laboratory of the University of California, Berkeley, while on leave of absence from Osaka University. From 1960 to 1970, he was an Associate Professor, and has been a Professor of Communication Engineering at Osaka University since 1971. He served as a Department Chairman in the periods of 1972–1973, 1977–1978, and 1983–1984. From 1980 to 1982, he was the Dean of Students of Osaka University. His fields of interest are electromagnetic theory, microwaves, millimeter-waves, and acoustic-waves engineering, optical fibers and optical fiber communication techniques, optical integrated circuits and devices, and lasers and their applications. He has published more than one hundred technical papers on these topics in established journals. He is the author or coauthor of several books, including *Microwave Circuits* and *Introduction to Relativistic Electromagnetic Field Theory*. From 1979 to 1981, he was Chairman of the Technical Group on the Microwave Theory and Techniques of the Institute of Electronics and Communication Engineers of Japan. He is Chairman of the Japan Broadcasting Corporation (NHK), Kinki Regional Broadcast Program Council, and a Consultant for the Nippon Telegraph and Telephone Public Corporation (NTT).

Dr. Kumagai is a member of the Institute of Electronics and Communication Engineers of Japan, the Institute of Electrical Engineers of Japan, and the Laser Society of Japan. He was awarded an IEEE Fellowship for contributions to the study of wave propagation in electromagnetics, optics, and acoustics.